View metadata, citation and similar papers at core.ac.uk
brought to you by CORE
provided by University of Queensland eSpace

Non-spherical optically trapped probes: design, control, and applications

J.A. Grieve[1], D.B. Phillips[1], S. Hanna[1], R.W. Bowman[2], G.M. Gibson[2], M.J. Padgett[2], M.J. Miles[1], D.M. Carberry[1,3], S.H. Simpson[1]

[1] H. H. Wills Physics Laboratory, University of Bristol, Bristol, United Kingdom
[2] SUPA, Department of Physics and Astronomy, University of Glasgow, Glasgow, United Kingdom
[3] Department of Physics and Mathematics, University of Queensland, Brisbane, Australia

ABSTRACT

In this proceedings paper we show describe how a microtool can be assembled, and tracked in three dimensions such that its full rotational and translational coordinates, $\boldsymbol{q}$, are recovered. This allows tracking of the motion of any arbitrary point, $\boldsymbol{d}$, on the microtool's surface. When the micro-tool is held using multiple optical traps the motion of such a point investigates the inside of an ellipsoidal volume – we term this a 'thermal ellipsoid. We demonstrate how the shape of this thermal ellipsoid may be controlled by varying the relative trapping power of the optical traps, and adjusting the angle at which the micro-tool is held relative to the focal plane. Our experimental results follow the trends derived by Simpson and Hanna.[1]

Keywords: Holographic Optical Tweezers, Nanotools, Microtools, Directed Assembly

1. INTRODUCTION

Since its inception in 1986,[2] the field of optical tweezing has grown to encompass a wide variety of optical micromanipulation techniques, with much interest focussed around the measurement of small (pN - fN scale) forces.[3] While most force measurement is achieved using optically trapped microspheres, the development of multiple-trap techniques such as holographic optical tweezers[4,5] and the generalised phase contrast method[6] enable the optical manipulation of non-spherical structures.

Repeated suggestion in the literature that high aspect ratio particles could play an important role as probes has resulted in an increased interest in characterising the motion and trapping properties of microrods. Several groups have demonstrated the capacity to trap and manipulate semiconducter,[7–10] polymer[11] and metal[12] nanorods using line traps and arrays of optical traps. The rotational modes resulting from the reduced symmetry of a rod when compared to a sphere have been the subject of numerous publications,[11,13] and a number of simulation works contribute to the growing literature on this topic.[14–16] The motion of an optically trapped microrod has been measured quantitatively by Phillips et al.,[17] with an active clamping technique proposed as a method of improving the resolution with which these structures can be positioned. On a smaller scale, bundles of carbon nanotubes have been trapped[18] and later used as Femtonewton force sensors by Marago et al.[19]

From among many potential uses for optically actuated micron-scale devices, the application of low-symmetry 'tools' as micron-scale force transducers is an emerging area of interest in the literature.[20–22] Tool structures potentially allow the removal of the interaction point from the laser foci, extending the reach of existing force sensing techniques to optically sensitive or opaque samples.[23] It is hoped that the ability to address a nanoscale interaction point by manipulating and observing micron-scale trapped structures will pave the way for higher resolution force-volume approaches, with the multiple 'handles' also allowing access to torque information.

Send correspondence to SHS, E-mail: stephen.simpson@bristol.ac.uk

Optical Trapping and Optical Micromanipulation IX, edited by Kishan Dholakia, Gabriel C. Spalding, Proc. of SPIE Vol. 8458, 84581Y · © 2012 SPIE · CCC code: 0277-786/12/$18 · doi: 10.1117/12.930871

Downloaded From: http://proceedings.spiedigitallibrary.org/ on 12/06/2015 Terms of Use: http://spiedigitallibrary.org/ss/TermsOfUse.aspx

2. EQUIPMENT

Holographic Optical Tweezers. Our HOT setup, similar what is reported in Gibson *et al*,[24] consists of a custom-made inverted microscope with a 1.4 NA, 100× objective (Plan-Neofluar, Zeiss), a closed-loop piezoelectric z postioner (Piezosystem Jena, Mipos 140 PL) for objective lens translations, and a motorized xy stage (MS-2000, ASI). The optical trap is powered by a Nd:YAG laser (Laser Quantum) emitting up to 3.2 W at 1064 nm. The beam is expanded to fill a spatial light modulator (Hamamatsu, X10468-07) and is imaged onto the back aperture of the objective lens. A polarizing beam splitter is used before the objective to transmit the laser beam while reflecting half of the illumination light onto a CCD camera (Microtron, MC). Image analysis and feedback control were implemented in LabVIEW (National Instruments)[25] running on a quad core PC. Hologram calculation was performed on the graphics processor unit (nVidia, Quadro FX 5600).

3. MICROTOOL ASSEMBLY

A key challenge in the emerging field of optically actuated probes is that of their fabrication. While conventional microsphere probes are widely available from a plethora of suppliers (for example, Bangs Laboratories and Corpuscular), with a variety of dimensions, materials and surface coatings, research involving microtools is still in its infancy and as yet there is no commerical source.

Several techniques to make microtools have been investigated, for example photolithographic techniques can be used to produce planar structures with feature sizes down to several hundred nanometres,[20] structures using two-photon polymerisation[22] and directed assembly of chemically-modified components.[21] We use the latter of these techniques to assemble the tools used in this paper. The components consist of: (i) biotin-coated high-aspect ratio silica microrods (diameter: 300 nm, length 20 μm), which are employed as probe tips or structural elements; and (ii) streptavidin-coated 2 μm silica microspheres, which are incorporated for their high affinity for optical manipulation and their well-understood trapping properties.

The biotinylation protocol used a two-stage functionalisation process. 3-Triethoxysilylpropylamine (APTES) was mixed with water in a 1:1 v/v ratio at a pH of 5, resulting in rapid hydrolisation. The pre-hydrolised APTES was then mixed with the microrods solution again at a 1:1 v/v concentraion, and incubated at room temperature for 15 minutes with constant agitation. Exposure to this silane compound produces a monolayer of amine-terminated molecules on the surface of the rods. Streptavidin coating of the carboxyl-terminated silica microspheres followed the traditional routes.

Probe assembly started with the adhesion of a single microsphere with a microrod. To accomplish this, once a rod and a sphere had been located and brought into the same working area in the sample chamber the trapped sphere was manipulated into contact with the rod by updating the position of its optical trap. Adhesion usually occurred within seconds, but additional time was allowed to facilitate the formation of additional biotin-streptavidin complexes, improving the bond rigidity. The process was repeated, attaching additional microspheres and microrods, to generate the required tools. Example tool designs are shown in Figure 1. For the experimental work analysis that follows, a tool comprising two microspheres and one rod was produced with the geometry, as indicated in Figure 1a.

4. THEORY OF MICROTOOL'S MOTION

The position of the tools is monitored by tracking the x, y, z coordinates of the microsphere 'handles'. When considering the forces experienced by the tool, we might naively consider these microspheres in isolation, as has been done in previous works.[21,26] This approach however produces confusing data, with as many separate force interactions as there are handles. Moreover, calibration of the microsphere handles is flawed if their coordinates are taken to be independent. We therefore introduce the concept of a 'generalised tool coordinate', defined as

$$\boldsymbol{q} = (\boldsymbol{r}, \boldsymbol{\theta}) \tag{1}$$

Where $\boldsymbol{r} = (r_x, r_y, r_z)$ and $\boldsymbol{\theta} = (\theta_x, \theta_y, \theta_z)$ represent translations of and rotations about the object's centre. Thus we are able to work with all six degrees of freedom available to a rigid object, and have a complete description of our system.

Downloaded From: http://proceedings.spiedigitallibrary.org/ on 12/06/2015 Terms of Use: http://spiedigitallibrary.org/ss/TermsOfUse.aspx

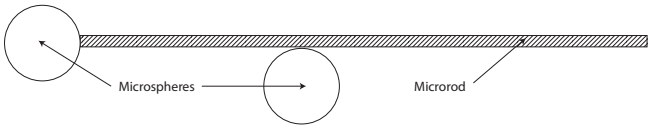

(a) Three-component, two handle

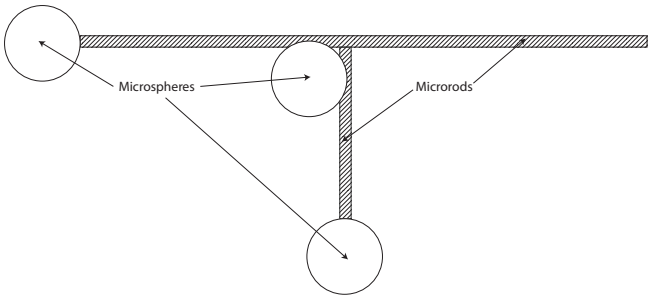

(b) Five-component, three handle

Figure 1. Schematic diagrams showing the design of probes with access to (a) five and (b) six degrees of freedom. Tools will be controlled via optical traps located over the microsphere 'handles', each of which will also act as a point of reference when tracking the position of the structure.

Using this set of coordinates, we can build analogs of the various one-dimensional equations governing the behaviour of microspheres. For example, the force experienced in a linear fluid flow $\boldsymbol{v}$ becomes

$$\boldsymbol{F} = \boldsymbol{\zeta}^t \boldsymbol{v}. \tag{2}$$

Similarly, the torque experienced by the tool in a circular flow $\boldsymbol{\omega}$ is given by

$$\boldsymbol{T} = \boldsymbol{\zeta}^r \boldsymbol{\omega} \tag{3}$$

where $\boldsymbol{\zeta}^t$ and $\boldsymbol{\zeta}^r$ are the translational and rotational hydrodynamic frictions of our tool. These quantities are 3×3 tensors, with off-diagonal terms implying the potential for coupling between orthogonal flows and forces/torques. Using the compound coordinate $\boldsymbol{q}$, we can generalise further to obtain

$$\begin{pmatrix} \boldsymbol{F} \\ \boldsymbol{T} \end{pmatrix} = \begin{pmatrix} \boldsymbol{\zeta}^t & \boldsymbol{\zeta}^c \\ (\boldsymbol{\zeta}^c)^T & \boldsymbol{\zeta}^r \end{pmatrix} \begin{pmatrix} \boldsymbol{v} \\ \boldsymbol{\omega} \end{pmatrix} \tag{4}$$

Here, $\boldsymbol{\zeta}^c$ is a pseudotensor representing potential coupling between rotational flows and forces, and linear flows and torques. These tensors indicate comparatively complex behaviour of these tools when compared with the simple microsphere.

4.1 The 3-Dimensional stiffness matrix

Like the friction matrix, the stiffness matrix relating displacements of the tool from its resting coordinates to forces and torques about its centre is a matrix quantity,[1] comprised of two tensors and two pseudotensors

$$\begin{pmatrix} \boldsymbol{F} \\ \boldsymbol{T} \end{pmatrix} = \begin{pmatrix} \boldsymbol{K}^t & \boldsymbol{K}^c \\ (\boldsymbol{K}^c)^T & \boldsymbol{K}^r \end{pmatrix} \boldsymbol{q} \tag{5}$$

Here $\boldsymbol{K}^t$ is interpreted as a tensor relating displacements of the probe centre to forces, $\boldsymbol{K}^r$ is a tensor relating rotations about the probe centre to torques, and $\boldsymbol{K}^c$ is a pseudotensor coupling rotations to forces and translations to torques. From this definition, we can see that the force experienced by the probe in, for example, the x direction is given by

Downloaded From: http://proceedings.spiedigitallibrary.org/ on 12/06/2015 Terms of Use: http://spiedigitallibrary.org/ss/TermsOfUse.aspx

$$F_x = xK^t_{xx} + yK^t_{xy} + zK^t_{zy} + \theta_x K^c_{xx} + \theta_y K^c_{xy} + \theta_z K^c_{xz} \tag{6}$$

In the case where $\boldsymbol{K}$ is perfectly diagonal, that is where all components K^t_{ij}, K^r_{ij} where $i \neq j$ are equal to zero as are all the components of $\boldsymbol{K}^c$, Equation 6 can then be rewritten $F_x = xK^t_{xx}$ and we have recovered the simple case where the forces can be treated independently. Note that the components of $\boldsymbol{K}$ may be positive or negative, provided that the net result of the forces and torques is to oppose the translation and rotation of the structure the conditions for confinement are satisfied.

It is useful to define how this matrix behaves under transformations of the coordinate frame. For rotations, each tensor and pseudotensor must be rotated separately, so for a rotation of the coordinate frame defined by the 3×3 rotation matrix $\boldsymbol{R}$, the rotated stiffness matrix $\boldsymbol{K'}$ is given by

$$\boldsymbol{K'} = \begin{pmatrix} \boldsymbol{R}\,\boldsymbol{K}^t\,\boldsymbol{R}^{-1} & \boldsymbol{R}\,\boldsymbol{K}^c\,\boldsymbol{R}^{-1} \\ \boldsymbol{R}\,(\boldsymbol{K}^c)^T\,\boldsymbol{R}^{-1} & \boldsymbol{R}\,\boldsymbol{K}^r\,\boldsymbol{R}^{-1} \end{pmatrix} \tag{7}$$

For translations of the coordinate system, it can be shown[1] that a shift in the coordinate system's origin by a vector $\boldsymbol{a}$ modifies the stiffness matrix such that

$$\boldsymbol{K}^t \rightarrow \boldsymbol{K}^{t\prime} = \boldsymbol{K}^t \tag{8a}$$

$$\boldsymbol{K}^c \rightarrow \boldsymbol{K}^{c\prime} = -(\boldsymbol{a} \times \boldsymbol{K}^t) + \boldsymbol{K}^c \tag{8b}$$

$$\boldsymbol{K}^r \rightarrow \boldsymbol{K}^{r\prime} = -(\boldsymbol{a} \times \boldsymbol{K}^t \times \boldsymbol{a}) - (\boldsymbol{a} \times (\boldsymbol{K}^c)^T) + (\boldsymbol{K}^c \times \boldsymbol{a}) + \boldsymbol{K}^r \tag{8c}$$

4.2 The optical stress centre

Analogous to the centre of gravity, for an object trapped in a three dimensional optical potential it is possible to define a point about which motion can be perfectly decomposed into translational and rotational modes. We term this point the *optical stress centre*.[1,27] In addition to its usefulness in understanding the modes of the system, measurement and manipulation of this stress centre may be used to tune the properties of a probe, potentially improving sensitivity in certain modes while maintaining confinement with respect to others.[28] When held far from any surfaces, the external potential on our tools is a function only of the position and power of the optical traps, so the optical stress centre can be measured in terms of the variance matrix or stiffness matrix (the two share properties making them interchangeable in this instance). Using the definition of $\boldsymbol{K}$ from Equation 5, it is the point about which the full matrix becomes symmetric.

The transformation of $\boldsymbol{K}^c$ when the coordinate frame is translated by a vector $\boldsymbol{a}$ is given by Equation 8b. This may be evaluated in terms of the components of $\boldsymbol{a}$ analytically, along with its transpose. When the coordinate frame is centred upon the optical stress centre, the condition

$$\boldsymbol{K}^c - (\boldsymbol{K}^c)^T = 0$$

is satisfied. Solving this for $\boldsymbol{a}$ we arrive at

$$\begin{pmatrix} a_x \\ a_y \\ a_z \end{pmatrix} = \begin{pmatrix} (K^t_{yy} + K^t_{zz}) & -K^t_{xy} & -K^t_{xz} \\ -K^t_{xy} & (K^t_{xx} + K^t_{zz}) & -K^t_{yz} \\ -K^t_{xz} & -K^t_{yz} & (K^t_{yy} + K^t_{xx}) \end{pmatrix}^{-1} \begin{pmatrix} K^c_{zy} - K^c_{yz} \\ K^c_{xz} - K^c_{zx} \\ K^c_{yx} - K^c_{xy} \end{pmatrix} \tag{9}$$

The vector $\boldsymbol{a}$ can now be interpreted as the displacement of the centre of the tool frame to the optical stress centre of the system. If however the external potential on the the tool is modified by another force, for example interaction with a near-by surface, this measured centre can no longer be considered the optical stress centre, and becomes a centre of rotation. This suggests a potential use in very low force sensing of surfaces (for example applications see Phillips *et al*[23]).

Downloaded From: http://proceedings.spiedigitallibrary.org/ on 12/06/2015 Terms of Use: http://spiedigitallibrary.org/ss/TermsOfUse.aspx

4.3 Equating the tool's coordinates

4.3.1 Five modes – two points in 3D

Extraction of the three translations in Cartesian space is accomplished by taking the mean r_x, r_y, r_z coordinates across the measured spheres.

$$\boldsymbol{r}_{COM} = \sum_{i=1}^{N} \frac{\boldsymbol{r}_i}{n} \tag{10}$$

Where N is the number of spheres monitored (here $N = 2$), and $\boldsymbol{r}_{COM}$ is the coordinate of the tool centre. This can be calculated for each point in a time series.

Extraction of the two accessible rotational modes can be accomplished in this specific case (two beads monitored) by a simple coordinate transformation. First, the vector defined by the two measured bead locations $\boldsymbol{r}$ is translated to the origin.

$$\boldsymbol{r} \rightarrow \boldsymbol{r}' = \boldsymbol{r}_1 - \boldsymbol{r}_0 \tag{11}$$

Where $\boldsymbol{r}_0$ and $\boldsymbol{r}_1$ are the measured coordinates of the two handles. The angles α, β representing the azimuthal and polar angle respectively are given by the spherical polar coordinate transformations

$$r = |\boldsymbol{r}| = \sqrt{r_x^2 + r_y^2 + r_z^2}; \tag{12a}$$

$$\alpha = \tan^{-1}(r_x/r_y); \tag{12b}$$

$$\beta = \cos^{-1}(r_z/|\boldsymbol{r}|) \tag{12c}$$

Where r_x, r_y, r_z are the three Cartesian components of $\boldsymbol{r}$.

4.3.2 Six modes – three or more points in 3D

Measurement of the six modes may be made if the tool lacks symmetry about any axis, and if we have measurements of more than two microsphere handles. The three modes representing translations of the tool's centre are trivially calculated as for the five DOF case using Equation 10. For the angular modes however, the three measured points describe more than one vector, and as such we cannot extract the angles using spherical polar coordinates. To recover these rotational modes, we adopt an approach based upon calculation of the principal axes of inertia of the ensemble.

Initially, the mean of the tool's centre of mass is calculated over a period in which the tool is considered 'at rest'. This position is then subtracted from the coordinates of the tool handles, and the moment of inertia of each point about the centre of mass may be calculated.

The moment of inertia tensor of the time-averaged positions of the tool handles $\boldsymbol{I}_{COM}$, is calculated using the general definition

$$\boldsymbol{I} = \begin{bmatrix} I_{11} & I_{12} & I_{13} \\ I_{21} & I_{22} & I_{23} \\ I_{31} & I_{32} & I_{33} \end{bmatrix} \tag{13}$$

Where

Downloaded From: http://proceedings.spiedigitallibrary.org/ on 12/06/2015 Terms of Use: http://spiedigitallibrary.org/ss/TermsOfUse.aspx

$$
\begin{aligned}
I_{11} = I_{xx} &= \sum_{k=1}^{N} m_k(y_k^2 + z_k^2) \\
I_{22} = I_{yy} &= \sum_{k=1}^{N} m_k(x_k^2 + z_k^2) \\
I_{33} = I_{zz} &= \sum_{k=1}^{N} m_k(x_k^2 + y_k^2) \\
I_{12} = I_{21} = I_{xy} = I_{yx} &= -\sum_{k=1}^{N} m_k x_k y_k \\
I_{13} = I_{31} = I_{xz} = I_{zx} &= -\sum_{k=1}^{N} m_k x_k z_k \\
I_{23} = I_{32} = I_{yz} = I_{zy} &= -\sum_{k=1}^{N} m_k y_k z_k
\end{aligned}
\tag{14}
$$

Here N is the number of points monitored and m_k is the mass centred at each point. As we are only interested in extracting orientations, it is sufficient that these masses be equal, thereby setting $m_k = 1$ for all k.

The moment of inertia tensor must now be diagonalised. This is achieved via eigendecomposition. The set of eigenvectors, q_i for $i = 1, 2, 3$ of the matrix, $\boldsymbol{I}$ and the corresponding eigenvalues, λ_i allow the construction of the factorised form

$$
\boldsymbol{I} = \boldsymbol{Q}\boldsymbol{\Lambda}\boldsymbol{Q}^{-1} \tag{15}
$$

Where $\boldsymbol{Q}$ is a matrix with its ith column equal to the eigenvector q_i and $\boldsymbol{\Lambda}$ is a diagonal matrix with $\Lambda_{ii} = \lambda_i$. Here $\boldsymbol{\Lambda}$ is the diagonalised form of $\boldsymbol{I}$, and $\boldsymbol{Q}$ is the rotation matrix that accomplishes this (the pre- and post-multiplication is characteristic of tensor rotation).

After diagonalisation, the rotation matrix $\boldsymbol{Q}$ is used to rotate the data into a 'tool frame'. At this point, the positions of the tool handles are used to produce instantaneous moment of inertia tensors $\boldsymbol{I}_i$ for the every measurement in the series. These are diagonalised via eigendecomposition as above, producing instantaneous rotation matrices $\boldsymbol{Q}_i$ such that

$$
\boldsymbol{Q}_i = \begin{pmatrix} 1 & -\theta_z^i & \theta_y^i \\ \theta_z^i & 1 & -\theta_x^i \\ -\theta_y^i & \theta_x^i & 1 \end{pmatrix} \tag{16}
$$

Where $\theta_x^i, \theta_y^i, \theta_z^i$ represent small, instantaneous rotations about x', y', z', the three orthogonal unit vectors making up the 'tool frame'. This algorithm for retrieving the rotational modes holds for small rotations about the tool frame, as Equation 16 relies on the small angle approximation. This condition will hold for most probe use, and is the motivation for the selection of tool axes by the algorithm. The orientation of the probe axes is selected as the frame that minimises rotations of the tool throughout the dataset. As such it is unlikely to coincide with the laboratory frame, or any 'intuitive' frame based on the perceived or intended orientation of the tool. To facilitate analysis of the mode data, it may be preferable to transform the modes to a third reference frame, setting (for example) the x axis as parallel to the tool's 'tip', and z parallel to the illumination axis. This may be accomplished using the rotation matrix $\boldsymbol{Q}$ from Equation 15.

Downloaded From: http://proceedings.spiedigitallibrary.org/ on 12/06/2015 Terms of Use: http://spiedigitallibrary.org/ss/TermsOfUse.aspx

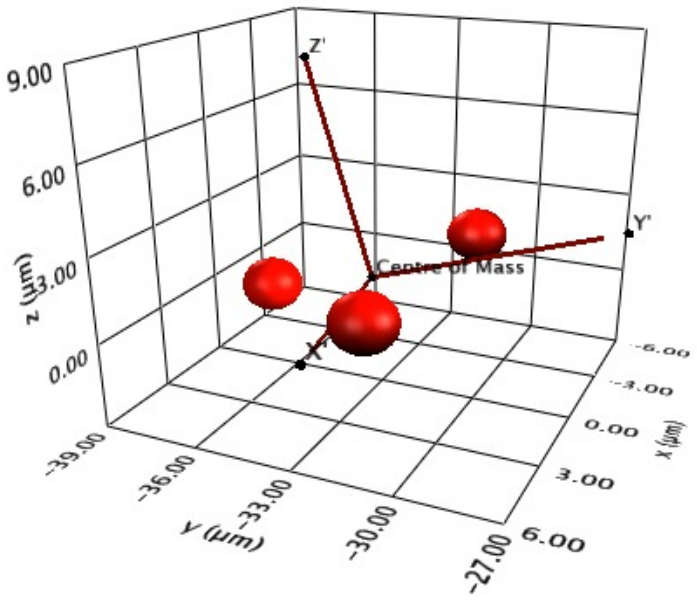

Figure 2. Example data showing the mean positions of the three handles comprising a low-symmetry tool in the laboratory frame (spheres are to scale, microrods connecting the spheres are not plotted). The origin and X', Y', Z' axes comprising the tool frame are also shown. Note that as expected the Z' axis is perpendicular to the plane defined by the tool handles. The X', Y' axes are positioned so as to minimise rotations in this frame.

5. MOTION OF THE PROBE TIP

The concept of a thermal volume is not new to the optical tweezers community. Optical tweezers have been used to implement a form of scanning probe microscopy known as 'photonic force microscopy' (PFM), in which a small sphere (typically ∼200 nm diameter) is optically trapped and tracked using a quadrant photodiode (QPD).[29] By observing the motion of the probe sphere, it is possible to map the three dimensional structure of a sample by identifying 'excluded volumes' – regions in which the sphere is not observed. In this way the thermal motion of the probe sphere is used as a sampling mechanism, with the optical tweezers' role reduced to the coarse positioning within the sample.[30] Using this technique, the internal structure of optically transparent samples may be imaged.

The thermal motion of a holographically trapped probe structure differs from that of a sphere. For locations away from the OSC, a 'thermal ellipsoid', the combination of a thermal disk (arising from rotations) and a spheroid (arising from translations)[1] describes the motion of any point on a hypothetical probe.

In general terms, the position of every point on the surface or within the volume of a rigid object is perfectly described by a 1×3 vector expressing its location with respect to the centre of the object, and the 1×6 vector $\boldsymbol{q} = (\boldsymbol{r}, \boldsymbol{\theta})$ representing the object's motion with respect to its translational modes ($\boldsymbol{r}$) and its rotational modes ($\boldsymbol{\theta}$).

While the 'five-component' tools discussed previously (see Figure 1) allow measurement of all six degrees of freedom, the 'three-component' tools experimentally investigated allow only five degrees of freedom to be measured, with rotation about the probe axis inaccessible. As such, only points along the probe axis are fixed perfectly in this way – any point 'off-axis' has a component of its position which is a function of the rotation about the probe axis.

Following Simpson and Hanna,[1] for any point $\boldsymbol{d}$ located at $\boldsymbol{a}$ (in the tool frame, with respect to the optical stress centre) with its location defined in this way, we may use measurements of the tool motion to extrapolate any properties which depend on position. For example, the variance may be extrapolated from the tool's stiffness matrix $\boldsymbol{K}$ using:

Downloaded From: http://proceedings.spiedigitallibrary.org/ on 12/06/2015 Terms of Use: http://spiedigitallibrary.org/ss/TermsOfUse.aspx

$$\langle \boldsymbol{d} \otimes \boldsymbol{d} \rangle = k_B T((\boldsymbol{K}^t)^{-1} - \boldsymbol{a} \times (\boldsymbol{K}^r)^{-1} \times \boldsymbol{a}) \tag{17}$$

5.1 Calculating the tip position

For each measurement of the generalised tool coordinate $\boldsymbol{q} = (\boldsymbol{r}, \boldsymbol{\theta})$, the corresponding tip position $\boldsymbol{d}$ can be calculated as

$$\boldsymbol{d} = \boldsymbol{R}(\boldsymbol{\theta})\boldsymbol{a} + \boldsymbol{r} \tag{18}$$

where $\boldsymbol{a}$ is the position of the tip with respect to the centre of the tool and $\boldsymbol{R}$ is a rotation matrix implementing rotations of θ_x, θ_y and θ_z about the x, y and z axes respectively. These rotations may be implemented sequentially such that $\boldsymbol{R}(\boldsymbol{\theta}) = \boldsymbol{R}_x(\theta_x)\boldsymbol{R}_y(\theta_y)\boldsymbol{R}_z(\theta_z)$. For a tool with only five degrees of freedom, θ_x is not recorded, so R_x is reduced to the identity matrix.

5.2 Measuring the thermal ellipsoid

The spatial distribution of the tip position forms a three dimensional ellipsoidal structure termed the 'thermal ellipsoid'. In order to characterise this volume, we first calculate its 3×3 variance matrix $\langle \boldsymbol{d} \otimes \boldsymbol{d} \rangle$. The variance matrix is then diagonalised by eigendecomposition, with the resulting eigenvalues defining the variance along the principle axes of the ellipsoid. The set of eigenvectors – arranged as a 3×3 matrix with the jth column corresponding to the jth eigenvector – defines the orientation of the ellipsoid.

An example three-dimensional scatter plot of a probe's tip position is shown in Figure 3, along with the calculated thermal ellipsoid. The plotted ellipsoid encloses two standard deviations of the population, corresponding to ∼95% of the plotted points.

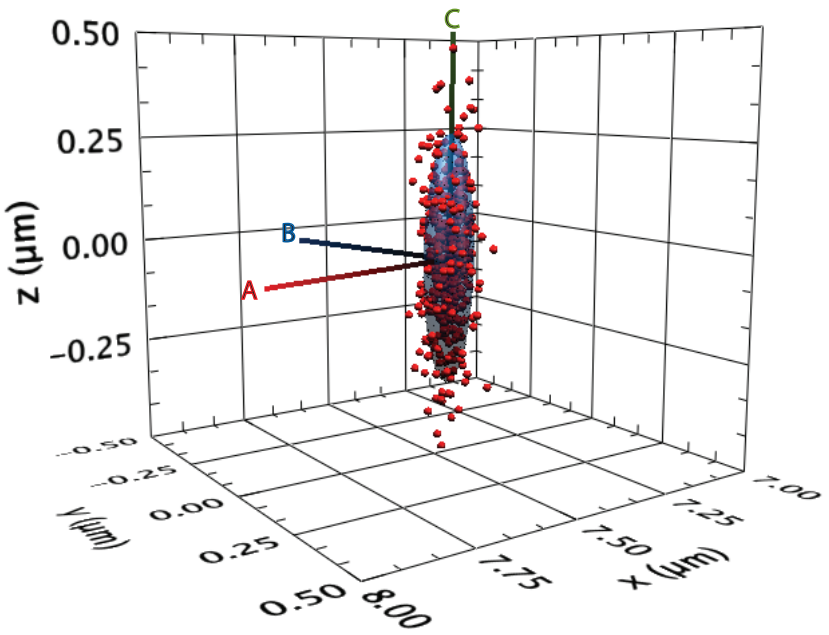

Figure 3. 3D scatter of the tip position with the thermal ellipsoid superimposed. The plotted ellipsoid has principle radii of twice the standard deviation measured parallel to the principle axes, and therefore encloses ∼95% of the plotted points. To better illustrate the orientation of the ellipsoid, the principle axes A, B and C are also plotted.

Figure 4(a) shows a sequence of ellipsoids, each representing two standard deviations of the position of the probe tip under a given translation of the optical stress centre (accomplished by varying the relative power between the optical traps). Ellipsoids are arranged in order of OSC location relative to the tip, with the ellipsoid corresponding to equal trap intensities indicated by an arrow. The lengths of the principle axes (corresponding to

Downloaded From: http://proceedings.spiedigitallibrary.org/ on 12/06/2015 Terms of Use: http://spiedigitallibrary.org/ss/TermsOfUse.aspx

one standard deviation) are plotted in Figure 4(b), along with the volume of the corresponding variance ellipsoid (i.e. the ellipsoid defined by the measured variance). We observe a wide plateau region, in which the volume does not change significantly (5.4 - 7.5 μm) with the volume rising rapidly outside this region. The thickness of the ellipsoid along its 'A' axis is relatively stable throughout the dataset. This direction corresponds closely to the laboratory x axis – parallel to the long axis of the probe and perpendicular to the 'thermal disk' resulting from rotations of the tool. As the total intensity in the traps is unchanged, the magnitude of the ellipsoid in this direction is not expected to vary. However, the standard deviations in the directions defined 'B' and 'C' (roughly corresponding to the laboratory y and z axes respectively) increase as the probe becomes less well confined, with the length 'C' most notably affected. This indicates that the principle contribution to the volume of the ellipsoid is the angular confinement of the probe.

For a single microsphere confined by an optical trap, the thermal motion describes a spheroid with its long axis parallel to the trapping axis (laboratory z). This is a condition imposed by the optical trap geometry, and cannot be altered without moving to a more complex geometry.[31,32] When a multi-component microtool is rotated out of the laboratory x, y plane, a corresponding rotation of the thermal ellipsoid described by the tip is predicted[1] predicted. To investigate this phenomenon, the data for a three-component probe initially oriented parallel to the laboratory x axis (before rotation about the laboratory y axis) is used to calculate thermal ellipsoids of the probe tip, with the results plotted in Figure 5. As in the previous figure, ellipsoid parameters (representing one standard deviation) are plotted, as is the ellipsoid volume (representing the tip variance). The orientation of the ellipsoid is also plotted, with rotation about the laboratory x and z axes showing no significant trend, and rotation about the y axis exhibiting positive correlation with the rotation of the tool, in qualitative agreement with the anticipated behaviour.

Figure 10 in Simpson and Hanna's paper,[1] plots ellipsoid parameters and volume against ϕ, the angle their hypothetical tool has been rotated about the y axis. Qualitatively, their a, c cross-sections agree well with ellipsoids calculated from experimental data, with the thermal volumes rotating with respect to the laboratory frame and 'thickening' (becoming less elongated). Agreement between the observed ellipsoids and the numerical model continues in the plot of the ellipsoid parameters, with the volume increasing and the ellipsoid becoming less elongated (an observed reduction in C, increase in A and B) as the tool is rotated.

In general, qualitative agreement with the predictions made by Simpson and Hanna regarding thermal volumes is good, with the distribution well described by an ellipsoid. The difference in the structure of the tools considered renders quantitative comparison impossible. However trends such as increasing tip volume with reduction in the relative trap intensity and rotation of the tool out of the x, y plane are observed in both systems.

For our experimental tools, the probe tip has been assumed to be on the axis. This is however unlikely to be the case due to the tool geometry. The tip is much more likely to be displaced by up to 2 μm from the axis, depending on the relative position of the microspheres on the rod. In this case, its position has a component which is a function of the rotation about the tool axis. While this rotation cannot be measured from the two points we are able to monitor, it is unlikely to be entirely unconstrained by the optical traps. Were this the case, it could be easily observed in the recorded images of the trapped probe. However there is likely to be a degree of variation in that angle, and as such we should expect the 'true' tip scatters to exhibit a degree of smearing in the y direction (for the data shown here).

6. CONCLUSIONS

To conclude, we have demonstrated the ability to exert some control over the size of the tip scatter by simple adjustment of the laser intensity incident upon the handles. This control could potentially be extended further, either by exploring more complex optical trap configurations or by examining a wider variety of tool designs. Modification of the relative stiffness of an optical trap in the axial direction has been demonstrated by Bowman et al.,[32] who reduce the effective numerical aperture of a holographically generated trap. It would be interesting to examine the effect this might have on a complex/extended structure.

We have also demonstrated the rotation of the thermal volume with respect to the trapping axis by simply rotating the microtool. It should also be possible to produce tool structures for which z motion of the 'tip' is constrained by the lateral trap stiffness of the tool handles, suggesting it may be possible to use composite

Downloaded From: http://proceedings.spiedigitallibrary.org/ on 12/06/2015 Terms of Use: http://spiedigitallibrary.org/ss/TermsOfUse.aspx

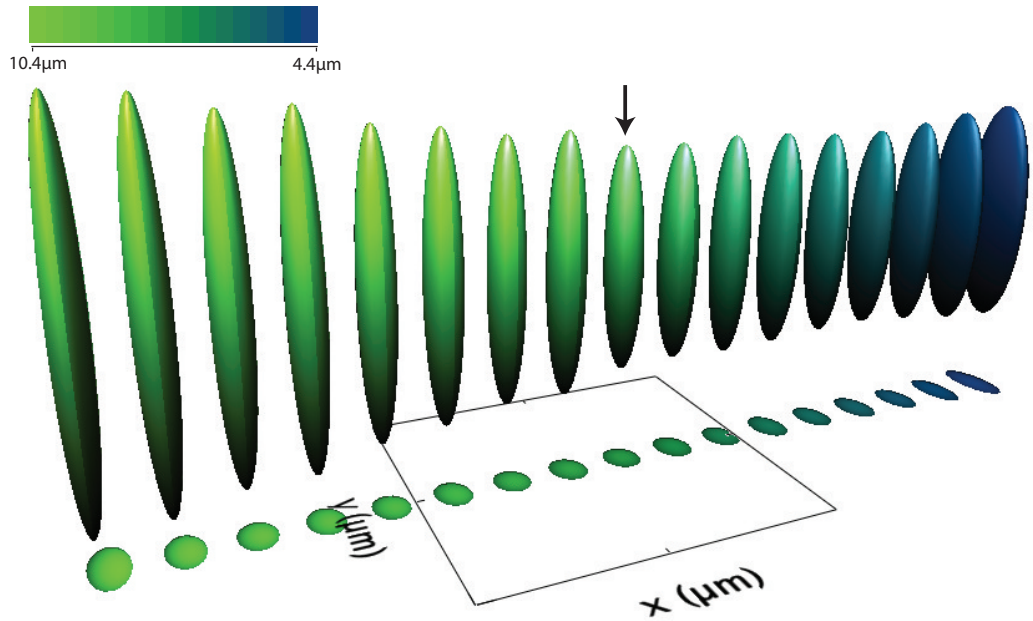

(a) Thermal ellipsoids

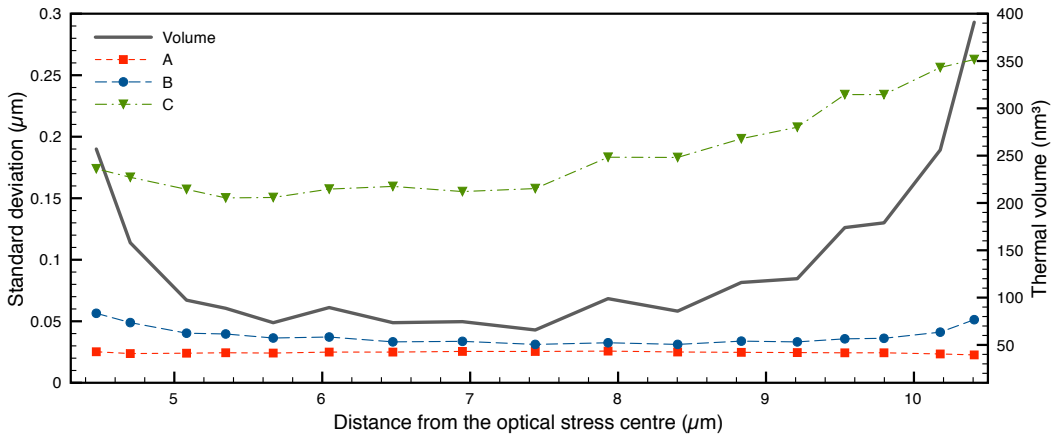

(b) Volume & parameters

Figure 4. Thermal ellipsoids for a three-component (two handle) tool as the optical stress centre is displaced. (a) Thermal ellipsoids representing two standard deviations of the thermal volume are plotted in the laboratory frame for a tool oriented parallel to the x axis as the optical stress centre is displaced (distance from the OSC is indicated by the color-bar). The ellipsoid corresponding to equal power in the tool 'handles' is indicated with an arrow. For scale a 1 μm^2 square is plotted. (b) The volume and ellipsoid parameters are plotted against the displacement of the tip from the optical stress centre. The volume exhibits a plateau over a $\sim$3 μm range, rising as the power moves to the extremes as this corresponds to the probe becoming trapped mostly by one handle.

Downloaded From: http://proceedings.spiedigitallibrary.org/ on 12/06/2015 Terms of Use: http://spiedigitallibrary.org/ss/TermsOfUse.aspx

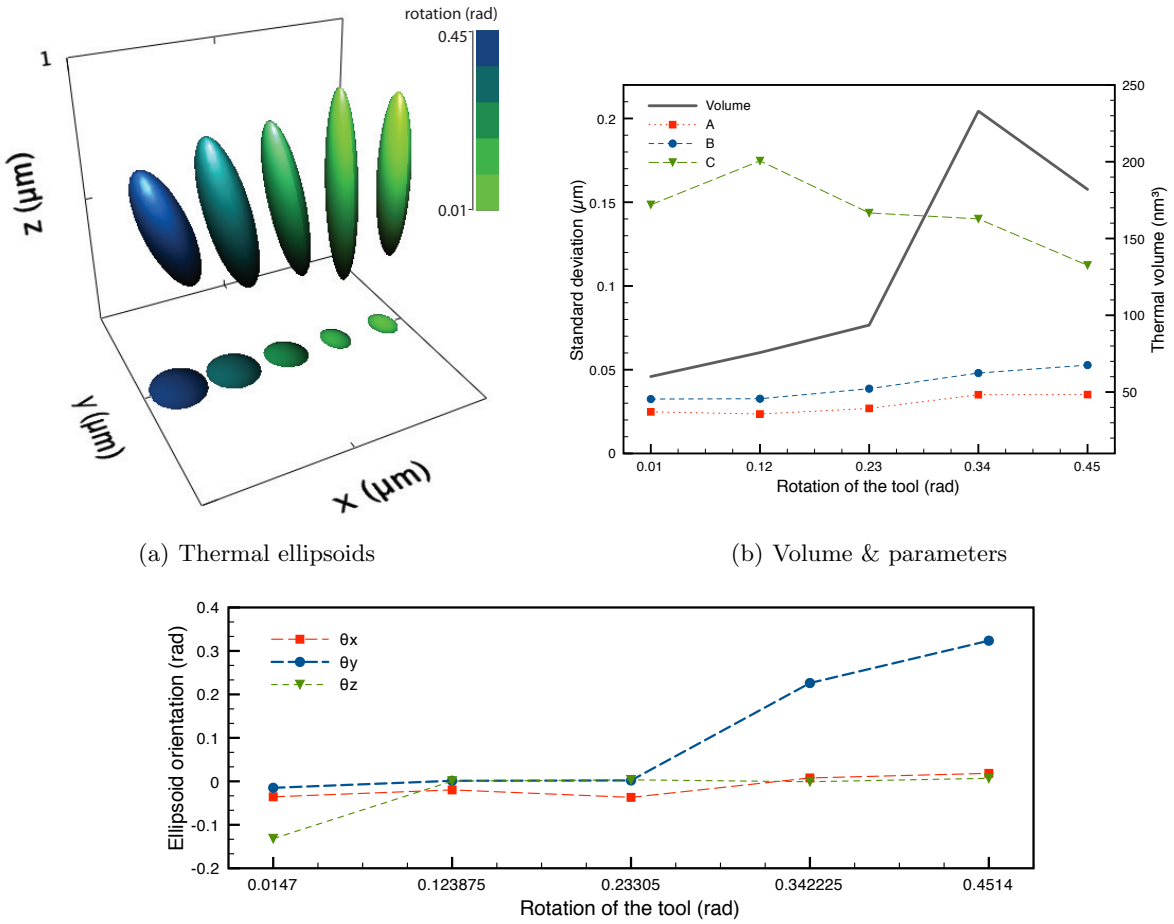

(a) Thermal ellipsoids

(b) Volume & parameters

(c) Ellipsoid orientation

Figure 5. Thermal ellipsoids for a three-component (two handle) tool as the tool is rotated out of the laboratory x, y plane. (a) Thermal ellipsoids representing two standard deviations of the thermal volume are plotted in the laboratory frame for a tool initially oriented parallel to the x axis as it is rotated about the y axis (the magnitude of rotation is indicated by the color-bar). For scale two faces of a $1\,\mu\text{m}^3$ cube are plotted. (b) The volume and ellipsoid parameters are plotted against rotation about the laboratory y axis. (c) shows the thermal ellipsoid orientation with respect to the laboratory axes. As the probe is rotated out of the x, y plane the volume increases, while the ellipsoid compresses (A and B increase while C decreases). This corresponds well with the predictions made by Simpson and Hanna (see *Figure 10* in[1]).

Downloaded From: http://proceedings.spiedigitallibrary.org/ on 12/06/2015 Terms of Use: http://spiedigitallibrary.org/ss/TermsOfUse.aspx

tools to produce thermal volumes which are not elongated in the direction of the trapping axis. As the thermal volume is of major significance in imaging techniques which make use of the Brownian motion as a scanning mechanism[30] this could be of interest in future imaging techniques employing optically trapped probes.

REFERENCES

[1] Simpson, S. H. and Hanna, S., "Thermal motion of a holographically trapped spm-like probe," *Nanotechnology* **20**(39), 395710 (2009).

[2] Ashkin, A., Dziedzic, J. M., Bjorkholm, J. E., and Chu, S., "Observation of a single-beam gradient force optical trap for dielectric particles," *Optics Letters* **11**(5), 288 (1986).

[3] Neuman, K. C. and Block, S. M., "Optical trapping," *Review of Scientific Instruments* **75**(9), 2787–2809 (2004).

[4] Reicherter, M., Haist, T., Wagemann, E. U., and Tiziani, H. J., "Optical particle trapping with computer-generated holograms written on a liquid-crystal display," *Optics Letters* **24**(9), 608–610 (1999).

[5] Curtis, J. E., Koss, B. A., and Grier, D. G., "Dynamic holographic optical tweezers," *Optics Communications* **207**(1-6), 169–175 (2002).

[6] Mogensen, P. C. and Glckstad, J., "Dynamic array generation and pattern formation for optical tweezers," *Optics Communications* **175**(13), 75–81 (2000).

[7] Bonin, K., Kourmanov, B., and Walker, T., "Light torque nanocontrol, nanomotors and nanorockers," *Optics Express* **10**(19), 984–989 (2002).

[8] Yu, T., Cheong, F.-C., and Sow, C.-H., "The manipulation and assembly of cuo nanorods with line optical tweezers," *Nanotechnology* **15**(12), 1732–1736 (2004).

[9] van der Horst, A., Campbell, A. I., van Vugt, L. K., Vanmaekelbergh, D. A., Dogterom, M., and van Blaaderen, A., "Manipulating metal-oxide nanowires using counter-propagating optical line tweezers," *Optics Express* **15**(18), 11629–11639 (2007).

[10] Lee, S.-W., Jo, G., Lee, T., and Lee, Y.-G., "Controlled assembly of in2o3 nanowires on electronic circuits using scanning optical tweezers," *Optics Express* **17**(20), 17491–17501 (2009).

[11] Neves, A. A. R., Camposeo, A., Pagliara, S., Saija, R., Borghese, F., Denti, P., Iat, M. A., Cingolani, R., Marag, O. M., and Pisignano, D., "Rotational dynamics of optically trapped nanofibers," *Optics Express* **18**(2), 822–830 (2010).

[12] Selhuber-Unkel, C., Zins, I., Schubert, O., Sonnichsen, C., and Oddershede, L. B., "Quantitative optical trapping of single gold nanorods," *Nano Letters* **8**(9), 2998–3003 (2008).

[13] Reece, P. J., Toe, W. J., Wang, F., Paiman, S., Gao, Q., Tan, H. H., and Jagadish, C., "Characterization of semiconductor nanowires using optical tweezers," *Nano Letters* **11**(6), 23752381 (2011).

[14] Jian, Y. C., Xiao, J. J., and Huang, J. P., "Optical force on dielectric nanorods coupled to a high-q photonic crystal nanocavity," *Journal of Physical Chemistry C* **113**(39), 17170–17175 (2009).

[15] Simpson, S. H. and Hanna, S., "Holographic optical trapping of microrods and nanowires," *Journal of the Optical Society of America A* **27**(6), 1255–1264 (2010).

[16] Simpson, S. H. and Hanna, S., "Optical trapping of microrods: variation with size and refractive index," *Journal of the Optical Society of America: A* **28**(5), 850–858 (2011).

[17] Phillips, D., Carberry, D., Simpson, S., Schafer, H., Steinhart, M., Bowman, R., Gibson, G., Padgett, M., Hanna, S., and Miles, M., "Optimising the optical trapping stiffness of holographically trapped microrods using high-speed video tracking," *Journal of Optics* **13**, 044023 (2011).

[18] Marago, O. M., Gucciardi, P. G., Bonaccorso, F., Calogero, G., Scardaci, V., Rozhin, A. G., Ferrari, A. C., Jones, P. H., Saija, R., Borghese, F., Denti, P., and Iati, M. A., "Optical trapping of carbon nanotubes," *Physica E: Low-dimensional Systems and Nanostructures* **40**(7), 2347–2351 (2008).

[19] Marago, O. M., Jones, P. H., Bonaccorso, F., Scardaci, V., Gucciardi, P. G., Rozhin, A. G., and Ferrari, A. C., "Femtonewton force sensing with optically trapped nanotubes," *Nano Letters* **8**(10), 3211–3216 (2008).

[20] Rodrigo, P. J., Gammelgaard, L., Bggild, P., Perch-Nielsen, I., and Glckstad, J., "Actuation of microfabricated tools using multiple gpc-based counterpropagating-beam traps," *Optics Express* **13**(18), 6899–6904 (2005).

Downloaded From: http://proceedings.spiedigitallibrary.org/ on 12/06/2015 Terms of Use: http://spiedigitallibrary.org/ss/TermsOfUse.aspx

[21] Ikin, L., Carberry, D. M., Gibson, G. M., Padgett, M. J., and Miles, M. J., "Assembly and force measurement with spm-like probes in holographic optical tweezers," *New Journal of Physics* **11**(2), 023012 (2009).

[22] Palima, D., Baas, A. R., Vizsnyiczai, G., Kelemen, L., Ormos, P., and Glckstad, J., "Wave-guided optical waveguides," *Optics Express* **20**(3), 2004–2014 (2012).

[23] Phillips, D., Grieve, J. A., Olof, S., Kocher, S., Bowman, R., Padgett, M. J., Miles, M. J., and Carberry, D. M., "Surface imaging using holographic optical tweezers," *Nanotechnology* **22**(28), 285503 (2011).

[24] Gibson, G., Carberry, D. M., Whyte, G., Leach, J., Courtial, J., Jackson, J. C., Robert, D., Miles, M., and Padgett, M., "Holographic assembly workstation for optical manipulation," *Journal of Optics A: Pure and Applied Optics* **10**(4), 044009 (2008).

[25] Gibson, G. M., Leach, J., Keen, S., Wright, A. J., and Padgett, M. J., "Measuring the accuracy of particle position and force in optical tweezers using high-speed video microscopy," *Optics Express* **16**(19), 14561–14570 (2008).

[26] Pollard, M. R., Botchway, S. W., Chichkov, B., Freeman, E., Halsall, R. N. J., Jenkins, D. W. K., Loader, I., Ovsianikov, A., Parker, A. W., Stevens, R., Turchetta, R., Ward, A. D., and Towrie, M., "Optically trapped probes with nanometer-scale tips for femto-newton force measurement," *New Journal of Physics* **12**(11), 113056 (2010).

[27] Carberry, D. M., Simpson, S. H., Grieve, J. A., Wang, Y., Schfer, H., Steinhart, M., Bowman, R., Gibson, G. M., Padgett, M. J., Hanna, S., and Miles, M. J., "Calibration of optically trapped nanotools," *Nanotechnology* **21**(17), 175501 (2010).

[28] Phillips, D. B., Simpson, S. H., Grieve, J. A., Gibson, G. M., Bowman, R., Padgett, M. J., Miles, M. J., and Carberry, D. M., "Position clamping of optically trapped microscopic non-spherical probes," *Optics Express* **19**(21), 20622–20627 (2011).

[29] Pralle, A., Florin, E.-L., Stelzer, E. H. K., and Hörber, J. K. H., "Photonic force microscopy: A new tool providing new methods to study membranes at the molecular level," *Single Molecules* **1**(2), 129–133 (2000).

[30] Tischer, C., Altmann, S., Fisinger, S., Hörber, J. K. H., Stelzer, E. H. K., and Florin, E.-L., "Three-dimensional thermal noise imaging," *Applied Physics Letters* **79**(23), 3878–3880 (2001).

[31] Singer, W., Bernet, S., Hecker, N., and Ritsch-Marte, M., "Three-dimensional force calibration of optical tweezers," *Journal of Modern Optics* **47**, 2921–2931 (2000).

[32] Bowman, R., Gibson, G., and Padgett, M., "Particle tracking stereomicroscopy in optical tweezers: Control of trap shape," *Optics Express* **18**(11), 11785–11790 (2010).

Downloaded From: http://proceedings.spiedigitallibrary.org/ on 12/06/2015 Terms of Use: http://spiedigitallibrary.org/ss/TermsOfUse.aspx